ACS APPLIED MATERIALS & INTERFACES

Letter

www.acsami.org

Cell Orientation Gradients on an Inverse Opal Substrate

Jie Lu,[†] Xin Zou,[†] Ze Zhao,[†] Zhongde Mu,[†] Yuanjin Zhao,*[,†,‡] and Zhongze Gu*[,†,‡]

[†]State Key Laboratory of Bioelectronics, School of Biological Science and Medical Engineering, Southeast University, Nanjing 210096, China

[‡]Laboratory of Environment and Biosafety Research Institute of Southeast University in Suzhou, Suzhou 215123, China

Supporting Information

ABSTRACT: The generation of cell gradients is critical for understanding many biological systems and realizing the unique functionality of many implanted biomaterials. However, most previous work can only control the gradient of cell density and this has no effect on the gradient of cell orientation, which has an important role in regulating the functions of many connecting tissues. Here, we report on a simple stretched inverse opal substrate for establishing desired cell orientation gradients. It was demonstrated that tendon fibroblasts on the stretched inverse opal gradient showed a corresponding alignment along with the elongation gradient of the substrate. This "random-to-aligned" cell gradient reproduces the insertion part of many connecting tissues, and thus, will have important applications in tissue engineering.

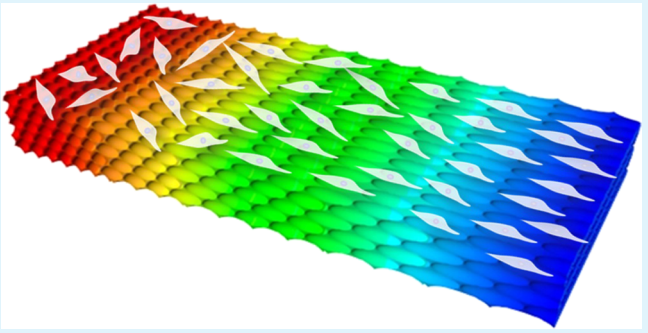

KEYWORDS: *cell gradient, inverse opal, colloidal crystal, cell orientation, biomaterial*

The phenomenon of cell gradients exists widely in biological systems, and plays an important role in guiding many biological processes, such as embryonic development and the interface integration of tissues.[1,2] Moreover, cell gradients are also important characteristics or requirements of some advanced biomaterials.[3−8] Therefore, the capability to generate biomimetic cell gradients is important for biological research.[9−12] To achieve this, several strategies have been employed to generate cell gradients through contact guidance by varying surface substrate properties, such as the density of polymer brushes, surface topography, surface wettability, stiffness of the substrate, and surface electrical cue.[13−16] However, most of these surfaces can only control the gradient of the cell density and have no effect on the gradient of the cell orientation, which also has an important role in regulating the functions of many connecting tissues, such as tendon-to-bone insertion sites and myotendinous junctions.[17,18] Thus, a novel method for the generation of cell orientation gradients is still anticipated for mimicking biological features.

Here, we propose a simple stretched inverse opal substrate for establishing the desired cell orientation gradients. It has been demonstrated previously that cells can grow in a certain orientation on substrates patterned with aligned fibrous, grooves, ridges or stretched inverse opals.[19−25] However, these substrates usually have a uniform surface morphology for uniformly inducing the cell orientation, and they cannot induce a change in gradient for cell morphology or cell orientation. Here, we propose a gradient stretching method to fabricate inverse opal substrates with elongation gradients on nanoscale-patterned structures traversing from one side of the substrate surface to the other. Cells cultured on these surfaces showed a controllable alignment along the direction of the elongation gradient of the substrate. In substrates with a lower degree of stretching, the cells assumed a random orientation. The degree of alignment increased with the increasing stretching ratio of the substrate. This random-to-aligned cell gradient reproduced the insertion part of many connecting tissues, and thus, will have important applications in tissue engineering.

In a typical experiment, the inverse opal substrates were fabricated using the vertical deposition method.[26−29] In this process, glass slides were first dipped vertically into an ethanol solution containing monodispersed SiO_2 nanoparticles. Colloidal crystal arrays of self-assembled SiO_2 nanoparticles were obtained after evaporation of the solution. To enhance the junction structures of the SiO_2 nanoparticles, we sintered the glass slides and the fabricated colloidal crystal arrays at 400 °C before the next fabrication step. The inverse opal structures were formed by filling the voids of the colloidal nanoparticle array templates with a polystyrene (PS)/toluene solution and evaporating the solvent to solidify the PS. To obtain a gradient stretching ratio within an inverse opal substrate, half of the film was heated to 80 °C in a water bath and stretched a given number of times its original length using a Vernier caliper. The junction structures were solidified by immersing the entire inverse opal substrate into cold water. Then, part of the stretched substrate was restretched again at 80 °C in a water

Received: April 1, 2015
Accepted: May 5, 2015
Published: May 5, 2015

DOI: 10.1021/acsami.5b02835
ACS Appl. Mater. Interfaces 2015, 7, 10091−10095

bath and then cooled in cold water. The same procedure was carried out to obtain a substrate that was stretched many times its original length (Figure 1). Thus, a gradual increase in the

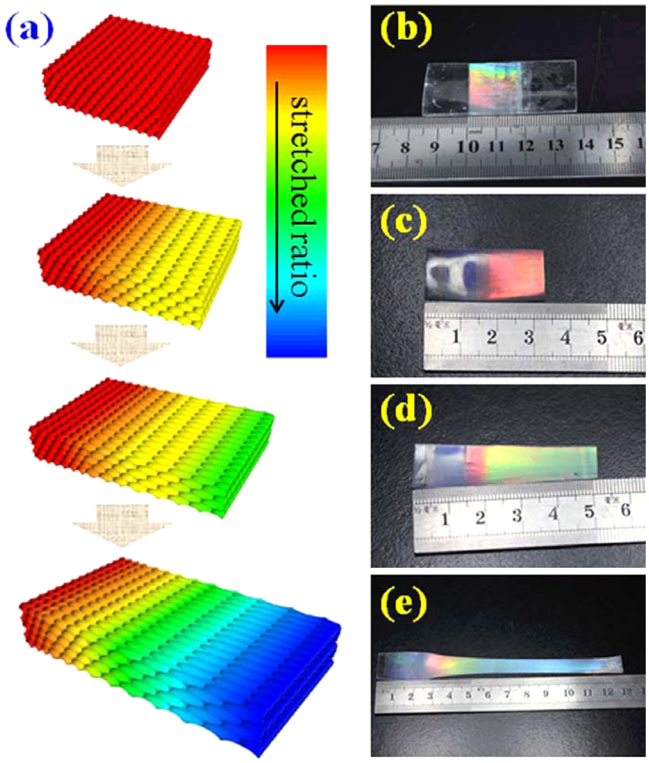

Figure 1. (a) Schematic diagram of the preparation of the stretched inverse opals with gradually increased stretching ratio, it did not correspond to b–e. (b–e) Images of inverse opal substrates with different stretching: (b) unstretched; (c) the combination of unstretched and 3 times stretched substrate; (d) the combination of unstretched, 3 times, and 6 times stretched substrate; (e) the combination of unstretched, 3 times, 6 times, and 12 times stretched substrate.

stretching ratio of the substrate could be achieved using this convenient approach, and an elongation of the gradient could be formed from one side of the substrate to the other within a single inverse opal substrate. From this method, different combinations of the stretching ratio could be obtained.

The microstructures of the gradient stretched inverse opal substrates were characterized using a scanning electron microscope (SEM). Different areas of the substrate were observed to investigate the change in gradient on the nanoscale (Figure 2a). The results are shown in Figures 2b–e. It was found that the continuous nanostructure of the inverse opal films was not damaged by the strain. However, over stretching would destroy the ordered structure of the elliptical pores on the substrates. (Figure S1 in the Supporting Information). The unstretched part of the inverse opal substrates maintained their three-dimensional ordered pore structure (Figure 2b). The ordered nanoporous structure changed from a round shape to an ellipse when viewed traversing from the unstretched side to the stretched side, which elongated from the round shape to approximately three times (Figure 2c), six times (Figure 2d), and 12 times their original length (Figure 2e). Thus, the gradient stretched inverse opal substrates displayed a gradual increase in the degree of porous orientation on their surfaces along the direction of stretching. As far as we are aware, this is the first report on the microstructure of this type of gradient surface. It was worth mentioning that although the surface inverse opal section was only about 2 μm thickness (Figure S2 in the Supporting Information), the whole substrate was more than 200 μm thickness before stretching and 50 μm thickness after stretching. With the stretching, the inverse opal scaffold became thin and thus its mechanics reduced. However, this surface was still rigid enough during the cell research.

To examine the effect of the gradient stretched inverse opal substrate on cells, rat tendon fibroblasts were cultured on the substrates to mimic the gradient structural organization of a tendon-to-bone insertion. Before culturing, the substrates were treated with O_2 plasma to increase their hydrophilic properties, and thus, encourage cell adhesion. After cell culture, a double staining using Calcein AM and Hoechst was carried out to visualize the actin cytoskeleton and nuclei of the tendon fibroblasts. Fluorescent images of the rat tendon fibroblasts cultured on the gradient stretched inverse opal substrates are shown in Figure 3. It can be seen that tendon fibroblasts on the unstretched part showed disordered microfilaments (Figure 3a). However, the cells exhibited a narrow angular distribution (Figure 3b) on the nearby surface having a moderate stretching ratio (about three times), and they exhibited a more uniform distribution (Figure 3c) on the part of the substrate with a stretching ratio of approximately six times. In particular, the cells cultured on the part with the highest stretching ratio (12 times) were spread widely along the longitudinal direction of the stretching, indicating an aligned orientation along the

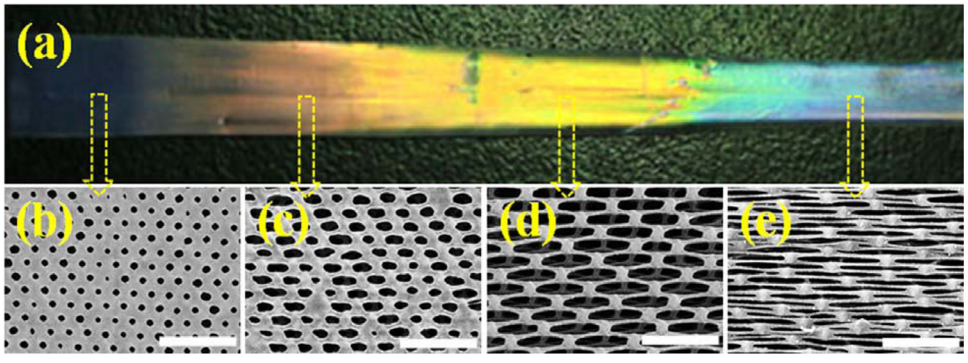

Figure 2. (a) Optical image of a gradient stretched inverse opal substrate, and (b–e) SEM images of the inverse opal substrate at different portions: (b) at unstretched portion; (c) at 3 times stretching portion; (d) at 6 times stretching portion; and (e) at 12 times stretching portion. Scale bars are 2 μm.

DOI: 10.1021/acsami.5b02835
ACS Appl. Mater. Interfaces 2015, 7, 10091–10095

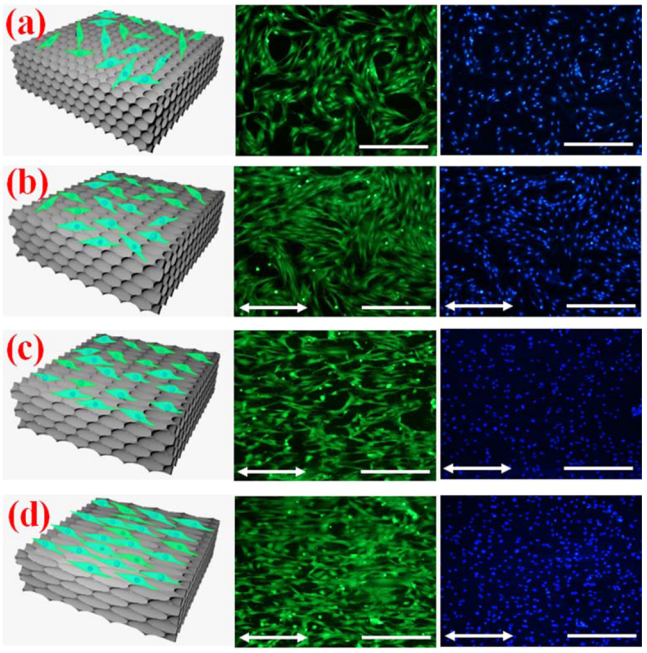

Figure 3. Schematic diagram and fluorescence microscopy images of tendon fibroblast cells cultured on a gradient stretched inverse opal substrate after 48 h: (a) on unstretched portion; (b) on 3 times stretched portion; (c) on 6 times stretched portion; and (d) on 12 times stretched portion. Green and blue fluorescence images are the cell cytoskeleton and nucleus, respectively. The double-sided arrows indicate the direction of stretching. Scale bar are 200 μm.

stretching direction (Figure 3d). The cell microfilaments were also elongated to the highest level and tight cell−cell connections were formed. Thus, tendon fibroblasts cultured on such surfaces exhibited an adjustable orientation on either the unstretched or stretched parts. It is worth noting that many different types of cells, such as HepG2 cells and NIH-3T3 cells, have also exhibited the adjustable orientation on the proposed substrate (Figure S3 in the Supporting Information). These cells remained their orientation until entering into cell apoptosis program.

The details of the tendon fibroblasts in different parts of the inverse opal scaffold were also investigated using SEM (Figure 4). The microstructure of the substrate was deformed because of the immersion in the culture media and the drying process used before capturing the SEM images. It can be seen that the fibroblasts cultured on the unstretched part of the inverse opal substrates exhibited disordered microfilaments (Figure 4a, e), and no specific orientation was observed. When the nanoscale structure changed from a round shape to 3 times stretched ellipse, a degree of uniform alignment was exhibited along the stretching direction (Figures 4b, f), and the tendon fibroblasts exhibited a higher degree of orientation compared with cells located on the unstretched part. Furthermore, cells showed a higher degree of orientation on 6 times stretched portion (Figure 4c, g). In particular, a significant degree of cell orientation was detected when the SEM probe focused on the area of the substrate that was stretched 12 times (Figure 4d, h). The fibroblasts showed a distinct alignment along the stretching direction compared with both the part with a lower stretching ratio and the unstretched part. This observation is consistent with the fluorescence results. Taken together, these results indicate that the nanoscale topography of the inverse opal substrates can affect the behavior of tendon cells, and the microfilaments of the tendon fibroblasts are able to sense the change in gradient of the inverse opal substrates. Thus, different orientations of tendon fibroblasts could be obtained on a single substrate, leading to the generation of random-to-aligned-oriented morphologies of the cells.

To qualify the orientation of the tendon fibroblasts in response to the gradient elongation of the inverse opal substrates, we analyzed the angle between the growth direction of the tendon fibroblasts and the stretching direction of the substrates (Figure 5a). The ImageJ software package was used to quantify the cell location relative to the stretching direction of the inverse opal scaffolds. In general, the orientation angle values were in the range 0−90°. An orientation angle of 0° represents parallel substrate stretching and cell orientation directions, which denote the long axis of the tendon fibroblasts. In contrast, an orientation angle of 90° represents an orientation perpendicular to the stretching direction. The cell numbers were counted for incremental orientation angle intervals of 30°. As shown in Figure 5b, the cell count in the orientation angle interval of 0−30° showed the highest alignment orientation number (92%) of the tendon fibroblasts on a surface with a stretching ratio of 12 times. Meanwhile, cells on the part of the substrate with a surface stretching ratio of six times showed a noticeably high alignment of 72%. A lower number of aligned cell orientations (37%) was found on the part of the substrate with a surface stretching ratio of three

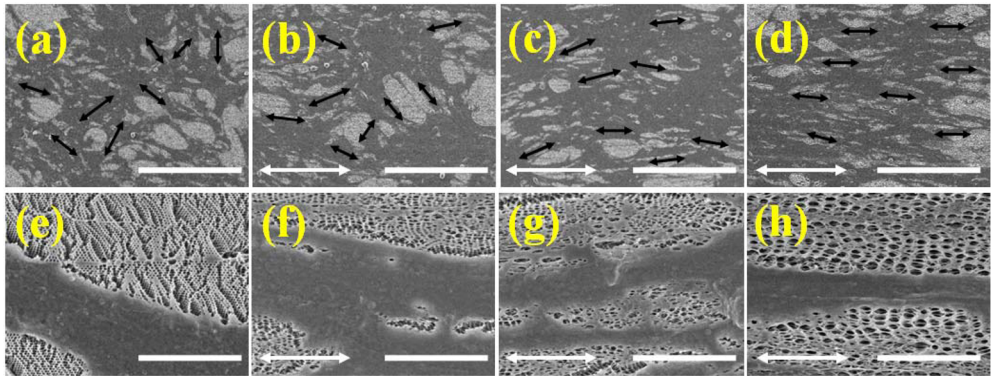

Figure 4. SEM images of tendon fibroblasts cultured on different portion of one substrate: (a) on unstretched portion; (b) on 3 times stretched portion; (c) on 6 times stretched portion and 12 times stretched portion; and (d) on 12 times stretched portion. (e−h) magnification images of a−d. Black arrows indicate cell orientation. White arrows indicate the direction of stretching. Scale bars are 200 μm in a−d and 20 μm in e−h.

DOI: 10.1021/acsami.5b02835
ACS Appl. Mater. Interfaces 2015, 7, 10091−10095

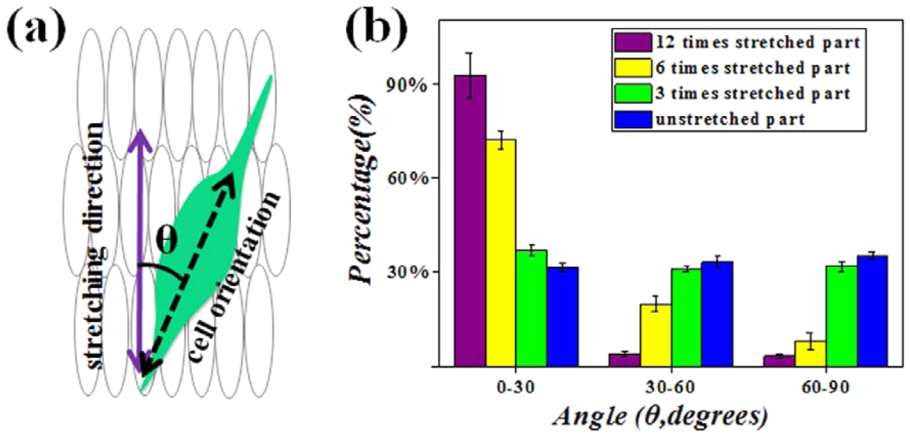

Figure 5. (a) Schematic of measuring the orientation angle; (b) Orientation angle frequency distribution of cells cultured on different portion of the stretched inverse opal substrate after 48 h. 500 cells in total were measured on each portion.

times. In contrast, no significant distribution in cell orientation was observed on the unstretched part of the substrate, corresponding with the fluorescent and SEM image data. Combining these observations, we believe that gradient stretching inverse opal substrates can induce different degrees of cell orientation.

In summary, we have demonstrated a simple approach to create random-to-aligned-oriented morphologies of cells that exist in many insertion tissues. Nanoscale inverse opal substrates with elongated gradients could be fabricated by simply introducing gradient stretching ratios in different parts of the substrates. Owing to an increasing aligned topography, random-to-aligned cell orientation gradients were easily formed on nanotopographical substrates without any chemical modification. These elongated gradient inverse opal substrates can also serve as useful platforms for generating different types of biomimetic cell gradients. Thus, it can be envisioned that these substrates will find important applications in tissue engineering and biological research.

EXPERIMENTAL SECTION

Materials. Monodisperse silicon dioxide spheres with diameters of 500 nm were laboratory homemade. PS, toluene solution, HF and glutaraldehyde were purchased from Aladdin, Shanghai, P. R. China. FBS without Mycoplasma, penicillin-streptomycin double antibiotics, DMEM medium and 0.25% Typin-EDTA was purchased from Gibco, USA. Dimethyl sulfoxide (DMSO) and Hoechst33342 were obtained from Sigma, USA. Calcein AM was purchased from molecular prober, USA. NIH-3T3 and HepG2 cells were purchased from Chinese Academy of Sciences.

Preparation of Inverse Opal Substrates. Opal film composed of monodisperse silica spheres was deposited on a glass by using vertical deposition method. After that, 20% PS/toluene solution was then infiltrated the opal template. The silica spheres were then etched with 4% HF after solidification of the solution hydrofluoric acid. Finally, the film was uniaxially stretched by Vernier caliper (Masterproof, Germany) to get different degrees elongation in an 80 °C water bath.

Rat Tendon Fibroblasts Extraction and Culturing. The tendon cells were harvested from rat supraspinatus and infraspinatus tendon samples. The tendon samples were first cut into small pieces and trypsinized for 5 min. To neutralize the trypsin activity, DMEM with 10% fetal bovine serum (FBS) were then added. After that, the tissue samples were placed in the incubator (HERA cell 150, Thermo, USA) at 37 °C and 5% CO_2 until fibroblasts migrated out and formed a confluent monolayer. The fibroblasts monolayer was then trypsinized and collected by centrifuging at 1000 rpm for 5 min. DMEM with 10% FBS were used to suspend the harvest tendon fibroblasts and cells were placed in the incubator for subculture. When grow to 80% confluence, cells with concentration of 2×10^3 cells/ml were then transferred to the wells (Thermo, USA) containing the inverse opal films. Medium was changed every day.

Characterization of Cells. For fluorescence images, double staining of Calcein AM and Hoechst were used to make the actin cytoskeleton and nuclear of tendon fibroblasts visualized. During the culture, the cells were stained by 10 μM Calcein AM and Hoechst33342 at 37 °C for about 15 min. Cells were then washed twice with PBS and observed by inverted fluorescence microscope (OLYMPUS IX71, Olympus, Japan). For SEM images, cell-loaded samples were washed with PBS before treat with 2.5% glutaraldehyde solution for 6 h at 4 °C. After treating, samples were dehydrated through alcohol of gradient concentrations. The concentration gradient of ethanol is 20, 40, 60, 80, to 100%, and each for 20 min. After that, the samples were imaged by SEM (S-3000N, Hitachi, Japan) after gold sputter coating.

ASSOCIATED CONTENT

Supporting Information

SEM images of the over stretched inverse opal substrate and the cross-section of an inverse opal substrate. Fluorescence microscopy images of HepG2 and NIH-3T3 cells cultured on unstretched and stretched inverse opal substrates, respectively. The Supporting Information is available free of charge on the ACS Publications website at DOI: 10.1021/acsami.5b02835.

AUTHOR INFORMATION

Corresponding Authors

*E-mail: yjzhao@seu.edu.cn.

*E-mail: gu@seu.edu.cn.

Notes

The authors declare no competing financial interest.

ACKNOWLEDGMENTS

This work was supported by the National Science Foundation of China (Grants 21473029, 91227124, and 21327902), the National Science Foundation of Jiangsu (Grants BK20140028 and BK20131293), the research Fund for the Doctoral Program of Higher Education of China (20120092130006), the Science and Technology Development Program of Suzhou (Grant ZXG2012021), the Program for Changjiang Scholars and Innovative Research Team in University (IRT1222), the Technology Invocation Team of Qinglan Project of Jiangsu Province, and the Program for New Century Excellent Talents in University.

DOI: 10.1021/acsami.5b02835
ACS Appl. Mater. Interfaces 2015, 7, 10091−10095

REFERENCES

(1) Gurdon, J. B.; Bourillot, P. Y. Morphogen Gradient Interpretation. *Nature* **2001**, *413*, 797−803.

(2) Zheng, W.-F.; Xie, Y.-Y.; Sun, K.; Wang, D.; Zhang, Y.; Wang, C.; Chen, Y.; Jiang, X.-Y. An On-Chip Study on the Influence of Geometrical Confinement and Chemical Gradient on Cell Polarity. *Biomicrofluidics* **2014**, *8*, 052010.

(3) O'Brien, F. J. Biomaterials & Scaffolds for Tissue Engineering. *Mater. Today* **2011**, *14*, 88−95.

(4) Yannas, I. V. Emerging Rules for Inducing Organ Regeneration. *Biomaterials* **2013**, *34*, 321−330.

(5) Zhao, Y.-J.; Cheng, Y.; Shang, L.-R.; Wang, J.; Xie, Z.-Y.; Gu, Z.-Z. Microfluidic Synthesis of Barcode Particles for Multiplex Assays. *Small* **2015**, *11*, 151−174.

(6) Li, Y.; Wang, S.-W.; Huang, R.; Huang, Z.; Hu, B.-F.; Zheng, W.-F.; Yang, G.; Jiang, X.-Y. Evaluation of the Effect of the Structure of Bacterial Cellulose on Full Thickness Skin Wound Repair on a Microfluidic Chip. *Biomacromolecules* **2015**, *16*, 780−789.

(7) Ding, B.; Chen, Z. Molecular Interactions between Cell Penetrating Peptide Pep-1 and Model Cell Membranes. *J. Phys. Chem. B* **2012**, *116*, 2545−2552.

(8) Cheng, Y.; Zheng, F.-Y.; Lu, J.; Shang, L.-R.; Xie, Z.-Y.; Zhao, Y.-J.; Cheng, Y.-P.; Gu, Z.-Z. Bio-Inspired Multicompartmental Microfibers from Microfluidics. *Adv. Mater.* **2014**, *26*, 5184−5190.

(9) Liu, W.; Shang, L.-R.; Zheng, F.-Y.; Qian, J.-L.; Lu, J.; Zhao, Y.-J.; Gu, Z.-Z. Photonic Crystal Encoded Microcarriers for Biomaterials Evaluation. *Small* **2014**, *10*, 88−93.

(10) Lipner, J.; Liu, W.; Liu, Y.; Boyle, J.; Genin, G. M.; Xia, Y.-N.; Thomopoulos, S. The Mechanics of PLGA Nanofiber Scaffolds with Biomimetic Gradients in Mineral for Tendon-to-Bone Repair. *J. Mech. Behav. Biomed. Mater.* **2014**, *40*, 59−68.

(11) Gurkan, U. A.; Assal, R. E.; Yildiz, S. E.; Sung, Y.; Trachtenberg, A. J.; Kuo, W. P.; Demirci, U. Engineering Anisotropic Biomimetic Fibrocartilage Microenvironment by Bioprinting Mesenchymal Stem Cells in Nanoliter Gel Droplets. *Mol. Pharmaceutics* **2014**, *11*, 2151−2159.

(12) Zheng, F.-Y.; Cheng, Y.; Wang, J.; Lu, J.; Zhang, B.; Zhao, Y.-J.; Gu, Z.-Z. Aptamer-Functionalized Barcode Particles for the Capture and Detection of Multiple Types of Circulating Tumor Cells. *Adv. Mater.* **2014**, *26*, 7333−7338.

(13) Christopher, J. B.; Robert, L.; Jeffrey, T. B. Engineering Substrate Topography at the Micro- and Nanoscale to Control Cell Function. *Angew. Chem., Int. Ed.* **2009**, *48*, 5406−5415.

(14) Katarina, W.; Regina, M.; Stefan, B.; Eva.-B, B.; Peter, F. Amoeboid Shape Change and Contact Guidance: T-Lymphocyte Crawling Through Fibrillar Collagen is Independent of Matrix Remodeling by MMPs and Other Proteases. *Blood* **2003**, *102*, 3262−3269.

(15) Yang, G.; Cao, Y.-H.; Fan, J.-B.; Liu, H.-L.; Zhang, F.-L.; Zhang, P.-C.; Huang, C.; Jiang, L.; Wang, S.-T. Rapid Generation of Cell Gradients by Utilizing Solely Nanotopographic Interactions on a Bio-Inert Glass Surface. *Angew. Chem.* **2014**, *126*, 2959−2962.

(16) Liu, W.-Y.; Zhang, Y.; Thomopoulos, S.; Xia, Y.-N. Generation of Controllable Gradients in Cell Density. *Angew. Chem., Int. Ed.* **2013**, *52*, 429−432.

(17) Xie, J. W.; Li, X.-R.; Lipner, J.; Manning, C. N.; Schwartz, A. G.; Thomopoulos, S.; Xia, Y.-N. Aligned-to-Random" Nanofiber Scaffolds for Mimicking the Structure of the Tendon-to-Bone Insertion Site. *Nanoscale* **2010**, *2*, 923−926.

(18) Yang, P. J.; Temenoff, J. S. Engineering Orthopedic Tissue Interfaces. *Tissue Eng. Part B* **2009**, *15*, 127−141.

(19) Brendon, M. B.; Albert, O. G.; Robert, B. M.; Ashwin, S. N.; Ross, A. M.; Jason, A. B.; Robert, L. M. The Potential to Improve Cell Infiltration in Composite Fiber-Aligned Electrospun Scaffolds by the Selective Removal of Sacrificial Fibers. *Biomaterials* **2008**, *29*, 2348−2358.

(20) Saha, S.; Duan, X.-R.; Wu, L.-Y.; Lo, P.-K.; Chen, H.; Wang, Q. Electrospun Fibrous Scaffolds Promote Breast Cancer Cell Alignment and Epithelial-Mesenchymal Transition. *Langmuir* **2012**, *28*, 2028−2034.

(21) Wang, Y.; Shi, H.; Qiao, J.; Tian, Y.; Wu, M.; Zhang, W.; Lin, Y.; Huang, Y. Electrospun Tubular Scaffold With Circumferentially Aligned Nanofibers for Regulating Smooth Muscle Cell Growth. *ACS Appl. Mater. Interfaces* **2014**, *6*, 2958−2962.

(22) Zhou, X.-T.; Hu, J.; Li, J.-J.; Shi, J.; Chen, Y. Patterning of Two-Level Topographic Cues for Observation of Competitive Guidance of Cell Alignment. *ACS Appl. Mater. Interfaces* **2012**, *4*, 3888−3892.

(23) Fujie, T.; Ahadian, S.; Liu, H.; Chang, H.-X.; Ostrovidov, S.; Wu, H.-K.; Bae, H.; Nakajima, K.; Kaji, H.; Khademhosseini, A. Engineered Nanomembranes for Directing Cellular Organization Toward Flexible Biodevices. *Nano Lett.* **2013**, *13*, 3185−3192.

(24) Lu, J.; Zheng, F.-Y.; Cheng, Y.; Ding, H.-B.; Zhao, Y.-J.; Gu, Z.-Z. Hybrid Inverse Opals for Regulating Cell Adhesion and Orientation. *Nanoscale* **2014**, *6*, 10650−10656.

(25) Qazi, T. H.; Mooney, D. J.; Pumberger, M.; Geißler, S.; Duda, G. N. Biomaterials Based Strategies for Skeletal Muscle Tissue Engineering: Existing Technologies and Future Trends. *Biomaterials* **2015**, *53*, 502−521.

(26) Li, H.; Wang, J.-X.; Pan, Z.-L.; Cui, L.-Y.; Xu, -L.; Wang, R.-M.; Song, Y.-L.; Jiang, L. Fabrication of Functional Colloidal Photonic Crystals Based on Well-Designed Latex Particles. *J. Mater. Chem.* **2011**, *21*, 14113−14126.

(27) Li, H.-L.; Wang, J.-X.; Yang, L.-M.; Song, Y.-L. Superoleophilic and Superhydrophobic Inverse Opals for Oil Sensors. *Adv. Funct. Mater.* **2008**, *28*, 3258−3264.

(28) Feng, L.-H.; Zhu, C.-L.; Yuan, H.-X.; Liu, L.-B.; Lv, F.-T.; Wang, S. Conjugated Polymer Nanoparticles: Preparation, Properties, Functionalization and Biological Applications. *Chem. Soc. Rev.* **2013**, *42*, 6620−6633.

(29) Wang, D.-Y.; Caruso, F. Lithium Niobate Inverse Opals Prepared by Templating Colloidal Crystals of Polyelectrolyte-Coated Spheres. *Adv. Mater.* **2003**, *15*, 205−210.

DOI: 10.1021/acsami.5b02835
ACS Appl. Mater. Interfaces 2015, 7, 10091−10095